Interfacial Dripping Faucet: Generating Monodisperse Liquid Lenses

Lorène Champougny,[1,2,*] Vincent Bertin,[3] Jacco H. Snoeijer,[3] and Javier Rodríguez-Rodríguez[1,2,†]

[1]Carlos III University of Madrid, Thermal and Fluids Engineering Department, Avenida de la Universidad, 30 (Sabatini building), 28911 Leganés (Madrid), Spain

[2]Carlos III University of Madrid, "Gregorio Millán Barbany" University Institute, Avenida de la Universidad, 30 (Sabatini building), 28911 Leganés (Madrid), Spain

[3]Physics of Fluids Group, Faculty of Science and Technology, University of Twente, 7500 AE Enschede, The Netherlands

(Received 2 January 2024; revised 5 September 2024; accepted 15 November 2024; published 17 December 2024)

We present a surface analog to a dripping faucet, where a viscous liquid slides down an immiscible meniscus. Periodic pinch-off of the dripping filament is observed, generating a succession of monodisperse floating lenses. We show that this interfacial dripping faucet can be described analogously to its single-phase counterpart, replacing surface tension by the spreading coefficient, and even undergoes a transition to a jetting regime. This liquid-liquid-gas system opens perspectives for the study of the dynamics of emulsions at interfaces.

DOI: 10.1103/PhysRevLett.133.254001

Since the times of J. C. Maxwell and Lord Rayleigh, the dripping faucet has attracted the attention of fluid mechanicists, applied mathematicians, and material scientists alike. Not only did it turn out to be a rich dynamical system—exhibiting behaviors such as period doubling, chaos, and dripping-to-jetting transition [1,2]—but also a very fruitful setting to study the fundamentals of liquid fragmentation [3]. In practice, the dripping faucet has served as a conceptual basis to develop tools for the generation of controlled liquid dispersions, either in air or in an immiscible liquid (emulsion). Techniques based on the dripping faucet are used in the pharmaceutical industry, micro- and nanotechnology, or metallurgy to produce monodisperse droplets with sizes ranging from several microns to around the millimeter [4].

Three-fluid dispersions (liquid/liquid/gas) are a common occurrence in food [5] and cosmetic products [6], coatings [7], as well as in separation [8,9] and cleaning processes [10–12]. In principle, techniques inspired from the dripping faucet can be applied to make dispersions involving more than two fluid phases—for example multiple emulsions for encapsulation [13], in which phases meet two by two. However, as soon as more than two immiscible phases meet, a triple contact line appears, thereby introducing a new ingredient with its own physics. Despite their practical interest, associated three-phase fluid systems are still sparsely understood. Recent advances include the shape of droplets sitting at the interface between an immiscible liquid and a gas [14,15]—commonly referred to as liquid lenses [16,17]—and their coalescence dynamics [18–20].

In this Letter we present a system analogous to the dripping faucet, where a dispersed phase made of liquid 2 is generated directly at the surface of an immiscible, denser liquid 1. We show that this original system, dubbed "interfacial dripping faucet," is able to periodically generate monodisperse liquid lenses in a controlled fashion, and we rationalize the volume of the produced lenses. This configuration provides a simple route for the generation of large collections of liquid lenses (emulsions at interfaces) but also offers a controlled setting to investigate pinch-off dynamics in the presence of a liquid/liquid/gas contact line.

System description—The interfacial dripping faucet geometry is sketched in Fig. 1 (see Fig. S2 in [21] for an experimental picture). A perfectly wetting vertical plate is partially dipped into a bath of liquid 1, which forms a meniscus. An injection needle placed vertically against the plate injects liquid 2 at a constant flow rate Q. Liquid 2 forms a rivulet flowing down the dry substrate until it meets the three-phase contact line between the plate and the meniscus of liquid 1. Downstream, a hanging ligament of liquid 2 forms at the surface of liquid 1. The fate of this ligament, of width w_0 at the contact line, depends on the liquid properties and flow conditions.

In our experiments, liquid 1 is ultrapure water, with density $\rho_1 = 998\ \mathrm{kg/m^3}$, dynamic viscosity $\mu_1 = 0.98$ mPa s, and surface tension $\sigma_{1a} = 72$ mN/m in our room conditions ($T = 21\,^{\circ}\mathrm{C}$). Six different alkanes and mineral oils, all lighter than water, are used as the dispersed phase (liquid 2). These liquids have similar densities ρ_2, surface tensions σ_{2a}, and interfacial tensions with water σ_{12}, but dynamic viscosities μ_2 spanning almost four decades (1.5 mPa s for dodecane to 7571 mPa s for mineral oil RTM30). The spreading parameter $\mathcal{S} = \sigma_{1a} - (\sigma_{12} + \sigma_{2a})$ of all those liquid pairs fulfills the condition $-2\ \min(\sigma_{2a}, \sigma_{12}) < \mathcal{S} < 0$, meaning that liquid 2 is able to form stable and uncloaked lenses on water [15,21].

Depending on the viscosity μ_2 and the injection flow rate Q of the dispersed phase, two regimes can be observed, as

*Contact author: lchampou@ing.uc3m.es

†Contact author: bubbles@ing.uc3m.es

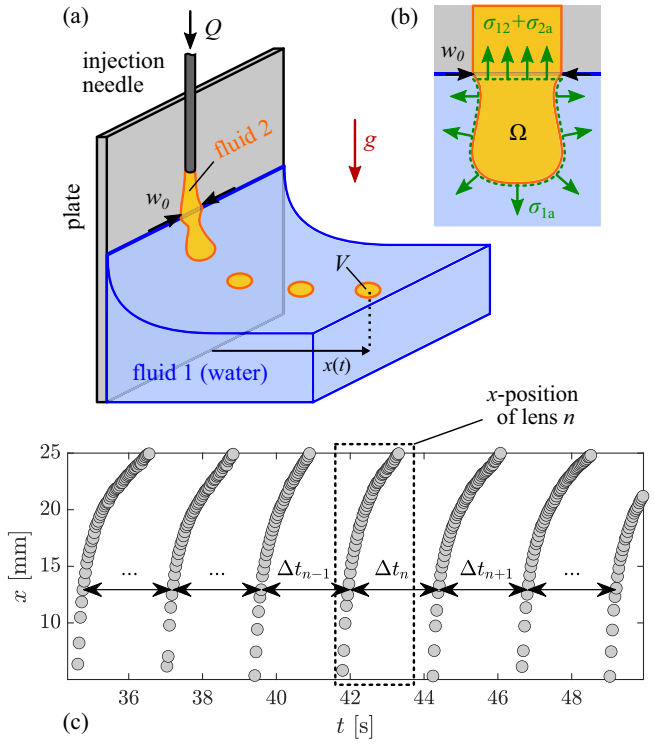

FIG. 1. (a) Geometry of the interfacial dripping faucet. (b) Capillary forces exerted on a control volume Ω of liquid 2, as it enters the meniscus region (blue). (c) Example of measured time evolution of the x position for consecutive lenses in the periodic pinch-off regime, allowing us to compute the dripping intervals Δt_n.

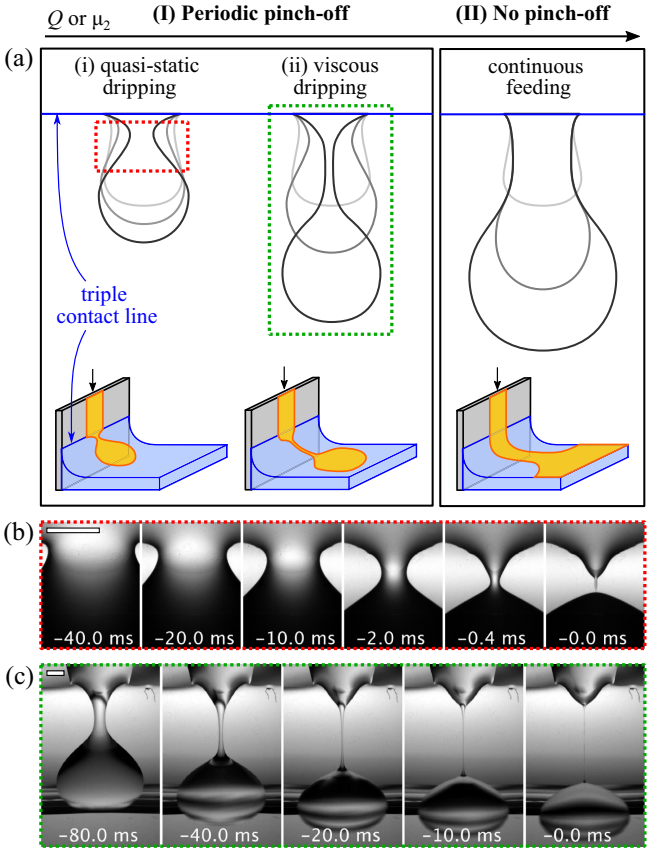

FIG. 2. (a) Regimes of the interfacial dripping faucet. The top sketches qualitatively represent the contour of the hanging ligament (front view) at different times, increasing from lighter to darker shade. The bottom sketches show a side view of the hanging ligament on the water meniscus. (b) Experimental time sequence of pinch-off for dodecane with $Q = 5$ μL/ min [quasi-static dripping, (i)]. (c) Time sequence of pinch-off for S200 mineral oil, $Q = 50$ μL/ min [viscous dripping, (ii)]. Both scale bars are 500 μm.

sketched in Fig. 2(a). In the first regime (I), found for small values of Q and/or μ_2, the hanging ligament of liquid 2 pinches off periodically, leading to the formation of identical liquid lenses that "drip" along the water meniscus (Movie S1). This periodic dripping regime remains stable as long as the injection continues, and the water surface is not entirely covered with lenses. High-speed imaging reveals that two limiting cases can be distinguished, depending on the pinch-off location and morphology. Quasistatic dripping (i) is characterized by a necking and pinch-off close to the contact line [Fig. 2(b), Movie S2]. In viscous dripping (ii), the hanging ligament stretches into a long thread that eventually pinches off further down on the meniscus [Fig. 2(c), Movie S3]. Increasing the flow rate Q and the viscosity μ_2 of liquid 2, another regime (II) emerges, in which the ligament never breaks (Movie S5).

Periodic pinch-off regime—We first focus on characterizing the periodic pinch-off regime (I). Experimentally we acquire videos of the meniscus region, where lenses are formed and break up from the hanging ligament. Once a lens has pinched off, its position x in the direction perpendicular to the plate is recorded as a function of time t using an automated in-house image processing code. Figure 1(c) displays examples of x-t trajectories of a series of lenses detached consecutively, here for dodecane injected at $Q = 50$ μL/ min. The time at which the lens reaches a reference position (∼13 mm in this case) allows us to robustly measure the time interval Δt_n between lens n and the following lens $n + 1$, referred to as the dripping interval. For a given liquid and flow rate, the average value Δt of the dripping intervals will be referred to as the dripping period [21]. In all our experiments, the typical variability in dripping interval is $\lesssim$10%, comparable to that of the classical dripping faucet in the constant-dripping interval regime [1]. Moreover, we do not observe any trend in these small fluctuations of Δt_n, which seem to be stochastic in nature [21]. We therefore treat the dripping period Δt as a well-defined observable for a given set of flow parameters.

When dripping is periodic, the volume V of the emitted lenses and the dripping period Δt are related by mass conservation, $Q = V\Delta t$. This relation holds as long as the volume of any satellite lens created at pinch-off can be neglected. Using high-speed recordings of the pinch-off, we

checked that the satellites are orders of magnitude smaller than the main lens, consistently with the observations of Ref. [30]. Figure 3(a) shows the lens volume V, deduced from the dripping period Δt, as a function of the flow rate Q for various injected liquids, color-coded according to their viscosity. We observe that the volume grows slowly with the flow rate for a given liquid, with a more pronounced slope the more viscous the liquid is. For a 250-fold increase in flow rate Q, the lens volume V grows by a factor 3 in the case of the least viscous liquid we studied (dodecane), and by a factor 5 for the much more viscous S200 mineral oil. To rationalize this behavior we propose a mechanistic model based on two key processes that must be completed for a lens to detach. First, the injected liquid accumulates at the plate-water-air contact line until a critical volume is reached, where capillary forces are no longer able to balance the weight of the hanging ligament. Then, liquid starts to drip and a second process starts: the ligament is stretched by a balance between gravity and elongational viscous stresses, until pinch-off eventually occurs. Let us now estimate the timescales of those two processes separately.

Analogously to pendant drops [31], there is a maximum volume V_c of liquid 2 that capillary forces can sustain against gravity in the interfacial dripping faucet. To determine V_c, we apply a force balance on a control volume Ω containing the injected liquid at the moment of lens detachment, highlighted by a dashed line in Fig. 1(b). The total capillary force exerted on Ω is $F_c \sim w_0(\sigma_{1a} - \sigma_{2a} - \sigma_{12}) = w_0\mathcal{S}$ [21]. Balancing F_c with the liquid weight in the hanging filament, $\rho_2 g V_c$ (where $g = 9.8\ \mathrm{m/s^2}$ is the acceleration of gravity) we find the critical volume $V_c \sim w_0|\mathcal{S}|/\rho_2 g$. In the limit where the flow rate Q and/or viscosity μ_2 are small enough (limit (i) in Fig. 2), V_c is expected to be a good estimate for the final detached lens volume. We thus denote the corresponding dripping period $\Delta t^{(\mathrm{i})} = V_c/Q$. Note that, to compute V_c, we treated the water-air surface—and thus the liquid ligament—as parallel to gravity. This assumption is valid as long as pinch-off occurs in the vicinity of the plate-water-air triple contact line, where the water meniscus is perfectly vertical thanks to the hydrophilic treatment applied to the plate. In our experiments, the typical lens size $V^{1/3}$ is smaller than the water meniscus extension, of order $\ell_{c1} = \sqrt{\sigma_{1a}/\rho_1 g}$, supporting the assumption of a vertical ligament ($0.4 \lesssim V^{1/3}/\ell_{c1} \lesssim 1$). Additionally, because the free surface of the meniscus is nearly vertical in the region where lenses form, buoyancy forces are approximately horizontal there [21], as these forces must be perpendicular to the water/air interface. This justifies neglecting buoyancy in the vertical force balance.

Once the critical volume is reached, the hanging ligament starts stretching under the action of gravity, with its motion resisted by viscous forces. Friction due to the water substrate can be neglected as $\mu_1 \ll \mu_2$ in most of our experiments, and the shear strain rate in the bath (of size $\sim$10 cm) is much smaller than the longitudinal strain rate inside the ligament (of millimetric length scale w_0). Viscous stresses are then dominated by the Trouton stresses inside the ligament, like in the viscous round jet [32], rather than by the shear stresses exerted by the bath on the ligament. Exact solutions have been obtained for the classical, axisymmetric dripping faucet [33], but we focus here on scaling arguments. Suppose that a viscous liquid starts to be injected at $t = 0$ from a nozzle of cross-sectional area A_0. At time t, the weight of liquid hanging is $\rho_2 g Q t$, which induces a stretching of the ligament that is mediated by viscosity. The elongational viscous stress is $3\mu_2\dot{\epsilon}$, where $\dot{\epsilon}$ is the stretching rate, and $3\mu_2$ the Trouton viscosity [34]. The corresponding viscous force in the ligament is $3\mu_2\dot{\epsilon}A \sim \mu_2 \partial A/\partial t$, where A is the instantaneous ligament cross section. Balancing this force with the lens weight, we find the typical stretching time of the ligament, $(\mu_2 A_0/\rho_2 g Q)^{1/2}$. For a large enough flow rate Q and/or viscosity μ_2 [limit (ii) in Fig. 2], we expect this stretching process to take much longer than reaching the critical volume V_c, therefore setting the dripping period, $\Delta t^{(\mathrm{ii})} = (\mu_2 A_0/\rho_2 g Q)^{1/2}$.

Most experiments actually lie between the two limits discussed previously. Since the quasistatic filling and viscous stretching steps occur in a mostly sequential manner (stretching starts only once V_c is reached), we propose to approximate the dripping period in the general case by the sum of the time taken by those two processes: $\Delta t = \Delta t^{(\mathrm{i})} + C\Delta t^{(\mathrm{ii})}$, with C a dimensionless numerical constant. This constant encapsulates the effect of the complex geometry of the ligament and cannot be determined solely by scaling arguments [21]. Such a constant is also needed in the equations used to predict the drop volume in the classical dripping faucet [35]. Multiplying the previous expression by Q/V_c, we arrive at

$$\frac{V}{V_c} = 1 + C(\mathrm{CaBo_2})^{1/2}. \tag{1}$$

We have introduced here the Bond number $\mathrm{Bo_2} = \rho_2 g w_0^2/|\mathcal{S}|$ of the hanging ligament, and the capillary number $\mathrm{Ca} = \mu_2 U/|\mathcal{S}|$ based on the characteristic injection speed at the contact line, $U = Q/A_0$. The cross-sectional area A_0 of the ligament is deduced from the experimental value of the ligament width w_0 and the wetting properties [21]. We show in [21] (section III-C) that the interpolation given by Eq. (1) is a good approximation to the exact solution derived by Wilson [33] for the vertical, axisymmetric dripping faucet.

Figure 3(b) shows the dimensionless volume V/V_c as a function of the dimensionless group $\mathrm{CaBo_2}$ for all the liquids used in our experiments. The color encodes the Ohnesorge number, $\mathrm{Oh} = \mu_2/\sqrt{\rho_2|\mathcal{S}|w_0}$. The experiments nearly collapse onto a master curve of the form given in Eq. (1) with a fitted constant $C = 8$ (solid line). The dotted line, corresponding to $C\ (\mathrm{CaBo_2})^{1/2} \sim 1$, qualitatively marks the transition from limiting behaviors (i) to (ii). We find the

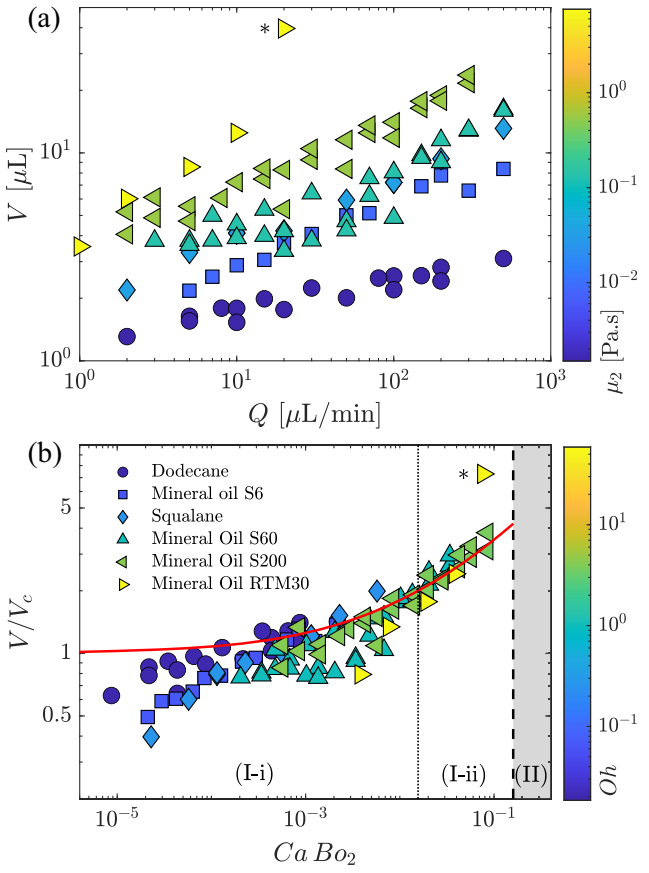

FIG. 3. (a) Average liquid lens volume, $V = Q\Delta t$, as a function of the flow rate Q. The color encodes the liquid dynamic viscosity μ_2. (b) Dimensionless lens volume V/V_c as a function of the dimensionless group CaBo_2. The color encodes the Ohnesorge number $\mathrm{Oh} = \mu_2/\sqrt{\rho_2 g w_0}$. The solid line corresponds to equation (1) with $C = 8$. The dotted and dashed lines show the transitions between periodic behaviors (i) and (ii), and between regimes (I) and (II), respectively. The asterisk highlights an experimental point where we observed that the ligament wobbles several times before eventually undergoing pinch-off.

collapse of the data quite remarkable, taking into account the simplifications of our model. First, the Ohnesorge number varies more than two orders of magnitude between the different liquids. Second, when changing liquids, not only does the Ohnesorge number change but also, to a lesser extent, the ligament wetting properties on water (i.e., Neumann angles) and the Bond number $\mathrm{Bo}_1 = w_0^2/\ell_{c1}^2$. In regime (I-i), the dimensionless data lies below the prediction of Eq. (1) and is slightly more scattered. This is to be expected since the precise value of the ratio $\psi = \lim_{\mathrm{CaBo}_2 \to 0} V/V_c$ must depend on the details of the geometry of the feeding ligament which, in turn, depend on the physical properties of the liquids. This is also true for the classical dripping faucet, where ψ can be as low as 0.6 [36]. For this reason, we do not leave ψ as a free parameter in Eq. (1), where it is assumed to be 1. Although the agreement with the experimental data would be quantitatively better, a single value of ψ should not formally be valid for all liquids. Moreover, allowing Eq. (1) to have two fitting parameters would conceal the good job that this equation does at fitting the experimental data over nearly four decades in the parameter CaBo_2. Instead, the reasonable agreement obtained with one fitting parameter shows the robustness of the underlying physical mechanisms.

No pinch-off regime—Increasing further the flow rate and viscosity of liquid 2, experiments show the emergence of another regime (denoted (II) in Fig. 2), in which the hanging ligament never breaks. Movie S4, corresponding to RTM30 and $Q = 20$ μL/ min, illustrates the transition towards pinch-off suppression: the ligament wobbles several times before eventually breaking. This delayed yet still periodic pinch-off translates into a very large lens volume (point marked with an asterisk in Fig. 3), which stands out of the experimental trend. Increasing further the flow rate (RTM30 and $Q = 50$ μL/ min), pinch-off is totally suppressed [gray area in Fig. 3(b)]. As illustrated in Movie S5, the ligament then continuously feeds a floating puddle of liquid 2 as long as injection continues.

We hypothesize the reason for the occurrence of regime (II) is that the water meniscus is curved, a fact that we ignored so far for the description of the periodic dripping regime (I). As a consequence of this curvature, the effective gravity felt by the ligament (i.e., the driving force promoting pinch-off) decreases as it slides down. If pinch-off has not occurred by the time the bath surface becomes horizontal and the driving force vanishes, then it never will. More quantitatively, the condition for the transition from regime (I) to (II) to happen is that the length ℓ_{po} at which the ligament would break exceeds the water meniscus length ℓ_{c1}. We can estimate the pinch-off distance as $\ell_{\mathrm{po}} \sim U t_{\mathrm{po}}$, with $t_{\mathrm{po}} \sim 6\pi\mu_2 w_0/|\mathcal{S}|$ the time taken by the stretched ligament to destabilize in the absence of gravity [21]. Thus, the condition $\ell_{c1} \sim \ell_{\mathrm{po}}$ for the onset of regime (II) is expressed as $6\pi \mathrm{CaBo}_1^{1/2} \sim 1$ or equivalently, $\mathrm{CaBo}_2 \sim \mathrm{Bo}_2/6\pi\mathrm{Bo}_1^{1/2} \approx 0.16$, roughly the same for all liquids. This threshold, plotted as a dashed line in Fig. 3(b), is consistent with the experimental data: $6\pi\mathrm{CaBo}_1^{1/2} = 0.45$ for the last point of periodic pinch-off (RTM30; $Q = 20$ μL/ min), and $6\pi\mathrm{CaBo}_1^{1/2} = 1.13$ for the first point of continuous feeding (RTM30; $Q = 50$ μL/ min).

Conclusion—In summary, we explore the physics of forced liquid dripping along an immiscible liquid/air interface, in partial wetting conditions. This three-phase configuration, dubbed "interfacial dripping faucet," exhibits a periodic pinch-off regime in a wide range of control parameters, leading to the generation of monodisperse liquid lenses. Both the critical volume and the dripping period are found to follow analogous laws to the free, axisymmetric dripping faucet [32,33], but with a key difference: the surface tension of the injected liquid must

be replaced by the spreading coefficient, $|\mathcal{S}|$. This accounts for the fact that the surface tension of the water-air interface does not contribute to keep a lens confined but, on the contrary, pulls to spread it. Beyond analogies, the interfacial dripping faucet also reveals an original regime not observed in a free vertical dripping faucet. For sufficiently large viscosity and flow rate of the dispersed phase, pinch-off is suppressed altogether and the liquid ligament continuously feeds a floating puddle.

A very important control parameter of the interfacial dripping faucet is the geometry of the meniscus, which is itself governed by the plate geometry and wettability. A steeper meniscus could translate into a delayed no-dripping regime, a thinner ligament (and hence smaller lenses), or even into the appearance of multiple dripping periods or a continuous jetting regime. The interfacial dripping faucet opens new perspectives to generate two-dimensional emulsions in the absence of confining walls [37,38] and, more generally, to study the fundamentals of liquid-liquid-gas dispersions, at play in many industrial and natural settings [5–12].

Acknowledgments—The authors acknowledge financial support from Grant No. PID2023-146809OB-I00 funded by MICIU/AEI/10.13039/501100011033 and by ERDF/UE (J. R.-R.), Grant No. PID2020-114945RB-C21 funded by MCIN/AEI/10.13039/501100011033 (J. R.-R. and L. C.), and VICI Grant No. 680-47-632 funded by NWO (V. B. and J. H. S.). This project has received funding from the European Union's Horizon 2020 research and innovation programme under the Marie Sklodowska-Curie Grant Agreement No. 882429 (L. C.).

[1] H. J. Subramani, H. K. Yeoh, R. Suryo, Q. Xu, B. Ambravaneswaran, and O. A. Basaran, Simplicity and complexity in a dripping faucet, Phys. Fluids **18**, 032106 (2006).
[2] C. Clanet and J. C. Lasheras, Transition from dripping to jetting, J. Fluid Mech. **383**, 307 (1999).
[3] J. Eggers and E. Villermaux, Physics of liquid jets, Rep. Prog. Phys. **71**, 036601 (2008).
[4] J. M. Montanero and A. M. Gañán-Calvo, Dripping, jetting and tip streaming, Rep. Prog. Phys. **83**, 097001 (2020).
[5] N. E. Hotrum, *Emulsion Droplet Spreading at Air/Water Interfaces: Mechanisms and Relevance to the Whipping of Cream*, Ph.D. Thesis, Wageningen University and Research, The Netherlands (2004).
[6] D. Venkataramani, A. Tsulaia, and S. Amin, Fundamentals and applications of particle stabilized emulsions in cosmetic formulations, Adv. Colloid Interface Sci. **283**, 102234 (2020).
[7] P. S. Purohit and P. Somasundaran, Modification of surface properties of cellulosic substrates by quaternized silicone emulsions, J. Colloid Interface Sci. **426**, 235 (2014).
[8] L. Su, Z. Xu, and J. Masliyah, Role of oily bubbles in enhancing bitumen flotation, Miner. Eng. **19**, 641 (2006).
[9] W. R. Rossen, Foams in enhanced oil recovery, in *Foams* (Routledge, New York, 2017), pp. 413–464.
[10] J. M. Shaw, A microscopic view of oil slick break-up and emulsion formation in breaking waves, Spill Sci. Technol. Bull. **8**, 491 (2003).
[11] I. D. Nissanka and P. D. Yapa, Calculation of oil droplet size distribution in ocean oil spills: A review, Mar. Pollut. Bull. **135**, 723 (2018).
[12] R. K. Gupta, G. J. Dunderdale, M. W. England, and A. Hozumi, Oil/water separation techniques: A review of recent progresses and future directions, J. Mater. Chem. A **5**, 16025 (2017).
[13] L.-Y. Chu, A. S. Utada, R. K. Shah, J.-W. Kim, and D. A. Weitz, Controllable monodisperse multiple emulsions, Angew. Chem. **46**, 8970 (2007).
[14] J. Sebilleau, Equilibrium thickness of large liquid lenses spreading over another liquid surface, Langmuir **29**, 12118 (2013).
[15] P. D. Ravazzoli, A. G. Gonzalez, J. A. Diez, and H. A. Stone, Buoyancy and capillary effects on floating liquid lenses, Phys. Rev. Fluids **5**, 073604 (2020).
[16] R. E. Johnson and S. S. Sadhal, Fluid mechanics of compound multiphase drops and bubbles, Annu. Rev. Fluid Mech. **17**, 289 (1985).
[17] A. Nepomnyashchy, Droplet on a liquid substrate: Wetting, dewetting, dynamics, instabilities, Curr. Opin. Colloid Interface Sci. **51**, 101398 (2021).
[18] M. A. Hack, W. Tewes, Q. Xie, C. Datt, K. Harth, J. Harting, and J. H. Snoeijer, Self-similar liquid lens coalescence, Phys. Rev. Lett. **124**, 194502 (2020).
[19] W. Tewes, M. A. Hack, C. Datt, G. G. Peng, and J. H. Snoeijer, Theory for the coalescence of viscous lenses, J. Fluid Mech. **928**, A11 (2021).
[20] T. Scheel, Q. Xie, M. Sega, and J. Harting, Viscous to inertial coalescence of liquid lenses: A lattice Boltzmann investigation, Phys. Rev. Fluids **8**, 074201 (2023).
[21] See Supplemental Material at http://link.aps.org/supplemental/10.1103/PhysRevLett.133.254001, which includes Refs. [22–29], for additional information about the experimental methods and a detailed discussion of the modeling.
[22] D. J. Luning Prak, S. M. Alexandre, J. S. Cowart, and P. C. Trulove, Density, viscosity, speed of sound, bulk modulus, surface tension, and flash point of binary mixtures of n-dodecane with 2, 2, 4, 6, 6-pentamethylheptane or 2, 2, 4, 4, 6, 8, 8-heptamethylnonane, J. Chem. Eng. Data **59**, 1334 (2014).
[23] A. Goebel and K. Lunkenheimer, Interfacial tension of the water/n-alkane interface, Langmuir **13**, 369 (1997).
[24] K. Takamura, H. Fischer, and N. R. Morrow, Physical properties of aqueous glycerol solutions, J. Pet. Sci. Eng. **98**, 50 (2012).
[25] V. I. Korotkovskii, A. Lebedev, O. Ryshkova, M. F. Bolotnikov, Y. E. Shevchenko, and Y. A. Neruchev, Thermophysical properties of liquid squalane C_30H_62 within the temperature range of 298.15–413.15 K at atmospheric pressure, High Temp. **50**, 471 (2012).
[26] M. J. Comuñas, X. Paredes, F. M. Gaciño, J. Fernández, J.-P. Bazile, C. Boned, J.-L. Daridon, G. Galliero, J. Pauly, K. R. Harris *et al.*, Reference correlation of the viscosity of squalane from 273 to 373 K at 0.1 MPa, J. Phys. Chem. Ref. Data **42** (2013).

[27] S. Goossens, D. Seveno, R. Rioboo, A. Vaillant, J. Conti, and J. De Coninck, Can we predict the spreading of a two-liquid system from the spreading of the corresponding liquid–air systems?, Langmuir **27**, 9866 (2011).
[28] P. Coullet, L. Mahadevan, and C. S. Riera, Hydrodynamical models for the chaotic dripping faucet, J. Fluid Mech. **526**, 1 (2005).
[29] R. Chandrasekhar, *Hydrodynamic and Hydromagnetic Stability* (Dover Publications, New York, 1981).
[30] J. C. Burton and P. Taborek, Role of dimensionality and axisymmetry in fluid pinch-off and coalescence, Phys. Rev. Lett. **98**, 224502 (2007).
[31] P.-G. Gennes, F. Brochard-Wyart, D. Quéré *et al.*, *Capillarity and Wetting Phenomena: Drops, Bubbles, Pearls, Waves* (Springer, New York, 2004).
[32] J. Eggers and T. F. Dupont, Drop formation in a one-dimensional approximation of the Navier–Stokes equation, J. Fluid Mech. **262**, 205 (1994).
[33] S. D. R. Wilson, The slow dripping of a viscous fluid, J. Fluid Mech. **190**, 561 (1988).
[34] P. Howell, *Extensional Thin Layer Flows* (University of Oxford, Mathematical Institute, 1994).
[35] R. Clift, J. Grace, and M. Weber, *Bubbles, Drops, and Particles*, Dover Civil and Mechanical Engineering Series (Dover Publications, New York, 2005).
[36] M. Wilkinson, Extended use of, and comments on, the drop-weight (drop-volume) technique for the determination of surface and interfacial tensions, J. Colloid Interface Sci. **40**, 14 (1972).
[37] K. W. Desmond, P. J. Young, D. Chen, and E. R. Weeks, Experimental study of forces between quasi-two-dimensional emulsion droplets near jamming, Soft Matter **9**, 3424 (2013).
[38] B. Dollet, A. Scagliarini, and M. Sbragaglia, Two-dimensional plastic flow of foams and emulsions in a channel: Experiments and lattice Boltzmann simulations, J. Fluid Mech. **766**, 556 (2015).